

University of Groningen

An observational and theoretical view of the radial distribution of H I gas in galaxies

Wang, Jing; Fu, Jian; Aumer, Michael; Kauffmann, Guinevere; Józsa, Gyula I. G.; Serra, Paolo; Huang, Mei-ling; Brinchmann, Jarle; van der Hulst, Thijs; Bigiel, Frank

Published in:
Monthly Notices of the Royal Astronomical Society

DOI:
[10.1093/mnras/stu649](https://doi.org/10.1093/mnras/stu649)

IMPORTANT NOTE: You are advised to consult the publisher's version (publisher's PDF) if you wish to cite from it. Please check the document version below.

Document Version
Publisher's PDF, also known as Version of record

Publication date:
2014

[Link to publication in University of Groningen/UMCG research database](#)

Citation for published version (APA):

Wang, J., Fu, J., Aumer, M., Kauffmann, G., Józsa, G. I. G., Serra, P., ... Bigiel, F. (2014). An observational and theoretical view of the radial distribution of H I gas in galaxies. *Monthly Notices of the Royal Astronomical Society*, 441(3), 2159-2172. <https://doi.org/10.1093/mnras/stu649>

Copyright

Other than for strictly personal use, it is not permitted to download or to forward/distribute the text or part of it without the consent of the author(s) and/or copyright holder(s), unless the work is under an open content license (like Creative Commons).

Take-down policy

If you believe that this document breaches copyright please contact us providing details, and we will remove access to the work immediately and investigate your claim.

Downloaded from the University of Groningen/UMCG research database (Pure): <http://www.rug.nl/research/portal>. For technical reasons the number of authors shown on this cover page is limited to 10 maximum.

An observational and theoretical view of the radial distribution of H I gas in galaxies

Jing Wang,^{1★} Jian Fu,² Michael Aumer,^{1,3} Guinevere Kauffmann,¹
Gyula I. G. Józsa,^{4,5} Paolo Serra,⁶ Mei-ling Huang,¹ Jarle Brinchmann,⁷
Thijs van der Hulst⁸ and Frank Bigiel⁹

¹Max–Planck–Institut für Astrophysik, Karl–Schwarzschild–Str. 1, D-85741 Garching, Germany

²Key Laboratory for Research in Galaxies and Cosmology, Shanghai Astronomical Observatory, CAS, 80 Nandan Rd, Shanghai 200030, China

³Excellence Cluster Universe, Boltzmannstr. 2, D-85748 Garching, Germany

⁴Netherlands Institute for Radio Astronomy (ASTRON), Postbus 2, NL-7990 AA Dwingeloo, the Netherlands

⁵Argelander-Institut für Astronomie, Auf dem H. gel 71, D-53121 Bonn, Germany

⁶Australia Telescope National Facility, CSIRO Astronomy and Space Science, PO box 76, Epping, NSW 1710, Australia

⁷Leiden Observatory, Leiden University, PO Box 9513, NL-2300 RA Leiden, the Netherlands

⁸University of Groningen, Kapteyn Astronomical Institute, Landleven 12, NL-9747 AD, Groningen, the Netherlands

⁹Institut für theoretische Astrophysik, Zentrum für Astronomie der Universität Heidelberg, Albert-Ueberle Str. 2, D-69120 Heidelberg, Germany

Accepted 2014 April 1. Received 2014 April 1; in original form 2014 January 13

ABSTRACT

We analyse the radial distribution of H I gas for 23 disc galaxies with unusually high H I content from the Bluedisk sample, along with a similar-sized sample of ‘normal’ galaxies. We propose an empirical model to fit the radial profile of the H I surface density, an exponential function with a depression near the centre. The radial H I surface density profiles are very homogeneous in the outer regions of the galaxy; the exponentially declining part of the profile has a scalelength of $\sim 0.18 R_1$, where R_1 is the radius where the column density of the H I is $1 M_{\odot} \text{pc}^{-2}$. This holds for all galaxies, independent of their stellar or H I mass. The homogeneous outer profiles, combined with the limited range in H I surface density in the non-exponential inner disc, results in the well-known tight relation between H I size and H I mass. By comparing the radial profiles of the H I-rich galaxies with those of the control systems, we deduce that in about half the galaxies, most of the excess gas lies outside the stellar disc, in the exponentially declining outer regions of the H I disc. In the other half, the excess is more centrally peaked. We compare our results with existing smoothed particle hydrodynamical simulations and semi-analytic models of disc galaxy formation in a Λ cold dark matter universe. Both the hydro simulations and the semi-analytic models reproduce the H I surface density profiles and the H I size–mass relation without further tuning of the simulation and model inputs. In the semi-analytic models, the universal shape of the outer H I radial profiles is a consequence of the *assumption* that infalling gas is always distributed exponentially.

Key words: galaxies: evolution – galaxies: ISM – galaxies: spiral.

1 INTRODUCTION

Over the last three decades, there have been many efforts to map the distribution of H I in galaxies using radio synthesis telescopes. The first analyses focused on massive and H I-luminous galaxies (e.g. Bosma 1978; Weavers et al. 1984). There were also surveys specifically focusing on galaxies in clusters (Warmels 1988; Cayatte et al. 1990; Verheijen & Sancisi 2001; Chung et al. 2009), which

demonstrated that the H I is depleted as a result of tidal stripping by neighbouring galaxies or ram-pressure stripping by the surrounding intracluster medium. Westerbork observations of neutral Hydrogen in Irregular and SPiral galaxies (WHISP; van der Hulst, van Albada & Sancisi 2001; Swaters et al. 2002) was one of the largest efforts to map the distribution of H I in different types of galaxies. The survey took nearly 10 years, observing around 500 galaxies with Hubble types from S0 to Im. From these studies, we have learned about the spatial and kinematic properties of H I in disc galaxies. The radial H I surface density profiles exhibit a wide variety of features attributable to irregularities in the galaxy such as spiral

★E-mail: hyacinthjing@gmail.com

arms, rings, bars, warps, etc. Studies of larger samples reveal basic scaling relations that provide hints of the mechanisms regulating the evolution of galaxies. In contrast to the stellar surface density, which is peaked in the centre of the galaxy and drops steeply with radius, the radial distribution of H I often flattens or even declines near the centre of the galaxy. In the outer regions, the H I discs usually extend to larger radius than the stellar discs and the profiles are well fitted by exponential functions. Studies of different types of galaxies reveal that they all obey the same tight H I size–mass relation (Broeils & Rhee 1997; Verheijen & Sancisi 2001; Swaters et al. 2002; Noordermeer et al. 2005). Recently, Bigiel & Blitz (2012, hereafter B12) found for a sample of 32 nearby spiral galaxies, that the combined H I and H₂ gas profiles exhibit a universal exponentially declining radial distribution, if the radius is scaled to R₂₅, the optical radius of the galaxies.

Recently, in an attempt to understand gas accretion in galaxies, we used the Westerbork Synthesis Radio Telescope (WSRT) to map hydrogen in a sample of 25 very gas rich galaxies, along with a similar-sized sample of ‘control’ galaxies with similar masses, sizes and redshifts (Wang et al. 2013, hereafter Paper I). Thanks to improvements in the WSRT instrumentation and data analysis, we were able to reach significantly lower H I column densities than previous surveys, which have targeted (late-type) disc galaxies in the field. The sample is selected using physical properties such as stellar mass and H I mass fraction, and is thus well suited for direct comparisons with theoretical models. In Paper I, we analysed the sizes and morphologies of the H I discs. The H I-rich galaxies lie on the extension of the well-known H I mass–size relation (Broeils & Rhee 1997) for normal spiral galaxies, and do not exhibit more irregular H I morphologies compared to the control galaxies. The conclusion is that major mergers are not likely to be the main source of the extra cold gas.

In this paper, we search for further clues about gas accretion by studying the radial H I surface density profiles of the galaxies in the sample. Again, we compare the H I-rich galaxies with the control sample. Our paper is organized as follows. Section 2 describes the data used in this paper. In Section 3, we present the radial profiles of H I and propose a model to describe the shape of the H I profiles. We present our major observational result that the galaxies exhibit a universal H I radial profile in the outer regions. In Section 4, we estimate H₂ profiles from the star formation rate (SFR) profiles for comparison with the results of B12. We compare our empirical results with smoothed particle hydrodynamics (SPH) simulations and semi-analytic models in Section 5. We discuss the possible physical origin of our main observational results in Section 6.

2 DATA AND PREVIOUS WORK

The Bluedisk project was designed to map the H I in a set of extremely H I-rich galaxies and a similar-sized set of control galaxies, which are closely matched in stellar mass, stellar mass surface density, inclination and redshift. The aim is to search for clues about how galaxy discs grow as a result of gas accretion in the local universe. We refer the readers to Paper I for details on the sample selection, observations and initial data analysis. Here, we review the most relevant information. All galaxies that were observed have stellar masses above $10^{10} M_{\odot}$, and redshifts between 0.01 and 0.03. All galaxies have optical photometry and spectroscopy from the Sloan Digital Sky Survey (SDSS; Abazajian et al. 2009) Data Release 7 spectroscopic MPA/JHU catalogue and ultraviolet (UV) photometry from the Data Release 5 of the *Galaxy Evolution Explorer* (GALEX) imaging survey (Martin et al. 2010). We have

gathered or measured a variety of parameters¹ describing the stellar component of the galaxies, including sizes (R₅₀ the half-light radius, R₉₀ the radius enclosing 90 per cent of the light, and D₂₅ the major axis of the ellipse where the *g*-band surface density reaches 25 mag arcsec⁻²), stellar mass (M_*), stellar mass surface density ($\mu_* = 0.5M_*/\pi R_{50}^2$), concentration index (R₉₀/R₅₀), colours and SFRs derived from spectral energy distribution fitting.

Following Paper I, the sample that will be used in this work includes 42 galaxies. Five interacting (multisource) systems, one strongly stripped system and one non-detection have been excluded. The analysis sample is divided into 23 H I-rich galaxies and 19 control galaxies, depending on whether the galaxy has more H I mass than deduced from its *NUV* – *r* colour and stellar mass surface density using the relation given in Catinella et al. (2010, hereafter C10). As in Paper I, our results are derived from the H I total intensity images, for which we have produced detection masks and error images. We have measured the size R₁ (the semimajor axis of the ellipse where the H I surface density reaches $1 M_{\odot} \text{pc}^{-2}$) for each galaxy. We have also parametrized the morphology of the H I discs using *A*, *M*₂₀ and *Gini* from the concentration–asymmetry–smoothness system (Conselice 2003; Lotz, Primack & Madau 2004), and three newly defined parameters that are more sensitive to irregularities in the outer parts of the H I discs, ΔCenter , ΔPA and ΔArea . The reader is referred to Paper I for more details.

3 A UNIVERSAL H I PROFILE

3.1 Derivation of the angular averaged radial surface density profiles

We measure the angular averaged radial H I surface density profile from total intensity images along ellipses with position angle and axis ratio (*a/b*) determined from the SDSS *r*-band images. The sampling radius (semimajor axis of ellipses) increases linearly with a step of 1 pixel (4 arcsec, ~ 2.8 kpc), which is smaller than the size of the synthesized beam in our data (~ 20 arcsec). We do not include the helium gas in our measurements except for the analysis in Section 4). We can typically measure the radial profiles out to an average surface density $\Sigma_{\text{H I}}$ of $0.2 \times 10^{20} \text{ atoms cm}^{-2}$. This limit is determined with the following considerations and tests.

(i) As described in Paper I, we used 4σ clipping to produce the H I intensity maps. We filter on multiple convolution scales so that the detection masks extend to include the faint emission. For the most sensitive filter (with a full width at half-maximum, FWHM, of 48 arcsec), we can detect emission with less than 25 km s^{-1} line width down to $0.2 \times 20 \text{ atoms cm}^{-2}$ at 4σ . We also check the clean-component images, and find that emissions are already detected at this surface density level.

(ii) We did a test by comparing the results from intensity maps with 3σ clipping and with 4σ clipping. The resulted profile shapes are very similar. This test and the last arguments ensure that we do not miss emission due to the clipping process when producing the total intensity images.

(iii) In Paper I, we also made error images for the total intensity images and estimated the depth of individual pixels (lim_{pix}) in the total intensity images. The depth of a radial profile can be estimated as $\text{sqrt}(2) \text{lim}_{\text{pixel}}/(2\pi R_1)$, where the factor of $\text{sqrt}(2)$ takes into account the fact that pixels are not independent (see the

¹ Please visit <http://www.mpa-garching.mpg.de/GASS/Bluedisk/data.php> for catalogues of optical and H I properties.

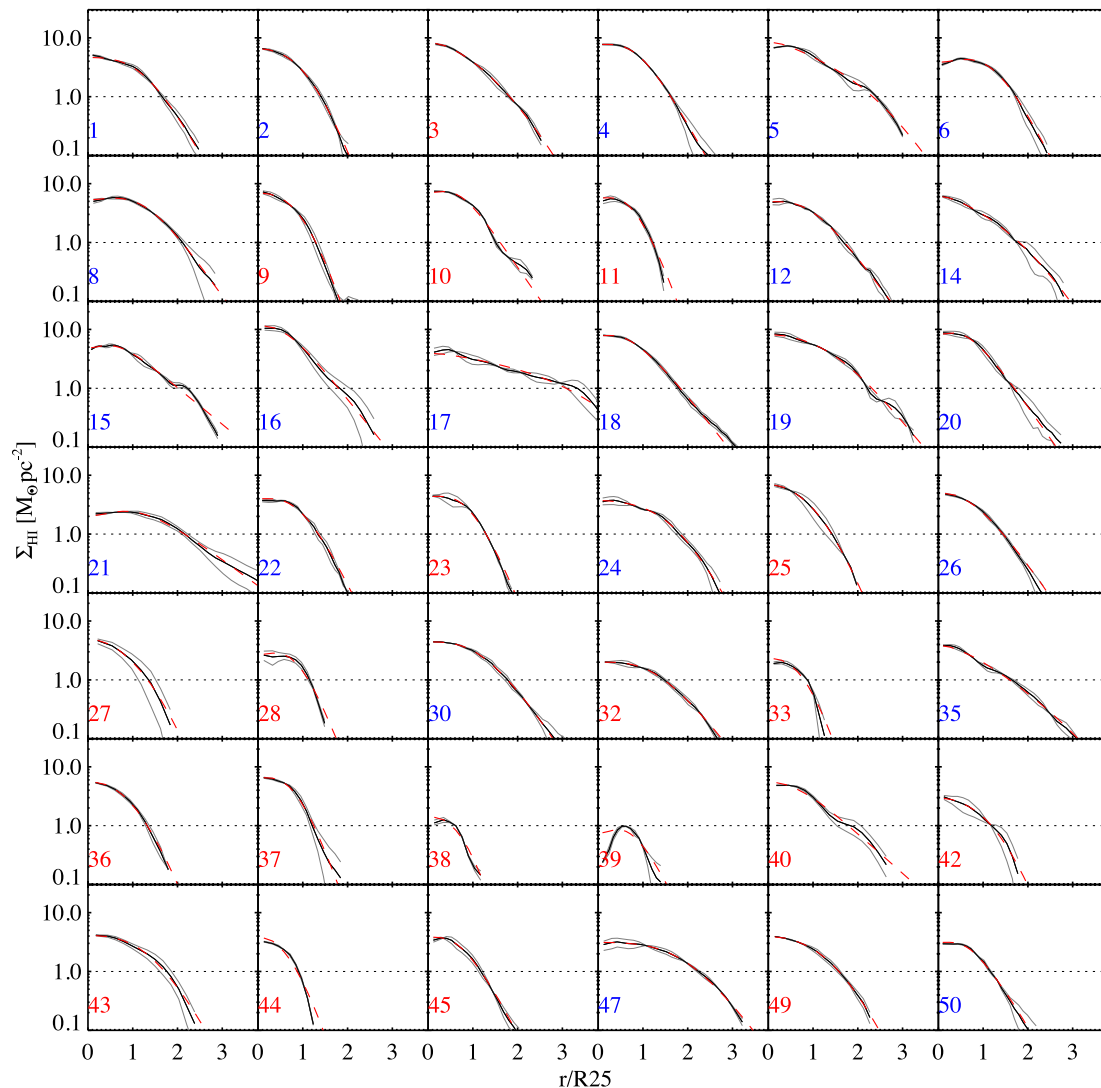


Figure 1. Radial profiles of the H I surface density for the 42 galaxies analysed in this paper. The azimuthally averaged profiles are plotted in black, the profiles for each half of the galaxy divided along the major axis are plotted in grey, and the best-fitting model fits (see Section 3.2) to the profiles shown in black are plotted as red dashed lines. Intersection of the profiles with the dotted lines indicate where the H I surface density reaches $1 M_{\odot} \text{pc}^{-2}$. The ID of each galaxy is noted in the corner, coloured in blue for H I-rich galaxies and in red for control galaxies.

appendix of Verheijen & Sancisi 2001). We get a maximum value of $0.15 \times 10^{20} \text{ cm}^{-2}$ for all the images, lower than the profile limit we use.

(iv) We also test by setting the profile limit to $0.5 \times 10^{20} \text{ atoms cm}^{-2}$, the results in the paper do not change.

The surface densities are corrected to be face-on by multiplying by $\cos\theta \sim b/a$, where θ is the inclination angle of the disc. We also divide the galaxy into two halves along the major axis and measure the radial H I surface density profile for each half. These profiles are displayed as one black and two grey curves in Fig. 1. We can see that the radial profiles for the two halves of the galaxy do not usually deviate much from the angular averaged radial profile, for both H I-rich and control galaxies. In the following sections, we only focus on the angular averaged H I radial surface density profiles (H I radial profiles for short hereafter). All the H I radial profiles decline exponentially in the outer regions and flatten or decline towards the central region, consistent with previous observations of nearby spiral galaxies (e.g. Wevers et al. 1984; Swaters et al. 2002).

3.2 Model fitting

It has often been remarked that the outer H I surface density profile follows an exponential form beyond the bright, star-forming stellar disc, while in the reach of the disc the surface density is more constant with a possible depression at the centre (e.g. Swaters et al. 2002; B12). To describe the shape of a two-component H I radial profile and to obtain the de-convolved shape of it, we choose a simple analytic expression of the form

$$\Sigma_{\text{H I, model}}(r) = \frac{I_1 \exp(-r/r_s)}{1 + I_2 * \exp(-r/r_c)}, \quad (1)$$

and fit our data to it, where I_1 , I_2 , r_s and r_c are free parameters. When the radius is large, the denominator is equal to 1 and the function reduces to an exponential with scale radius r_s . r_c is the characteristic radius where the profile transitions to the inner flat region. Because the H I+H2 gas exhibits an exponential radial distribution (see B12, and Section 4 in this paper), I_1 is related to the H I+H2 gas and I_2 is related to the H I/H2 ratio at $r = 0$ (see also Leroy et al. 2008). A similar formula was proposed by Obreschkow

et al. (2009), with r_c fixed to $0.63 r_s$. As we will show below, this model is very suitable to describe the radial distribution of H I surface density under the resolution of Bluedisk type.

We use the IDL code MPFIT (Markwardt 2009), which performs least-squares curve and surface fitting. To achieve a fast and stable fit, the whole fitting procedure includes three steps.

(i) The first step is to guess the initial value of the model parameters. We ignore the angular distribution of H I surface density in the H I image and the convolution effect of the beam, and simply perform a linear fit to the outer half of the H I radial profile. The slope and intercept distance of the linear fit are converted into initial guesses for r_s and I_1 . The initial r_c is set equal to $0.9 r_s$ and the initial I_2 is set equal to 9; these are the mean values of these parameters found by Leroy et al. (2008).

(ii) In the second step, we assume both the H I surface density distribution and the beam are azimuthally symmetric. With the initial parameters obtained in the last step, we build a model profile and convolve it with one-dimensional Gaussian function with a width of FWHM $\sim \sqrt{b_{\min} \times b_{\max}}$, where b_{\min} and b_{\max} are the minor and major axis (in FWHM) of the beam. The convolved profile ($\Sigma_{\text{H I, model}}$) is compared with the observed profile. The MPFIT code then tunes the model parameters to find the best fit.

(iii) In the final step, we take into account the axis ratio and position angle of both the galaxy and the beam in the H I image. The best-fitting model parameters from the second step are used as initial input. We build a model image with the observed axis ratio and position angle of the galaxy. The model image is then convolved with the beam. We measure the radial profiles ($\Sigma_{\text{H I, model}}$) from the convolved model image in the same way as they are measured from the observed H I image (Section 3.1). The simulated profiles are compared to the observed H I radial profile. The MPFIT code is then used to tune the model parameters to find the best fit.

The best-fitting model profiles are displayed as red dashed lines in Fig. 1. We can see that in general the model describes the observed profiles very well.

We now estimate errors for our derived parameters, as well as degeneracies in the fits. We construct a grid around the best-fitting parameters: r_s and r_c vary with a step size of $0.02 R_{25}$ in a range $\pm R_{25}$ about the best-fitting values, while I_1 and I_2 vary with step size of 0.01 dex in a range ± 1 dex about the best values. We calculate the sum of square residuals between the convolved model and the data at each grid point

$$\kappa^2 = \sum \left(\frac{(\Sigma_{\text{H I, model}} - \Sigma_{\text{H I}})^2}{\sigma(\Sigma_{\text{H I}})^2} \right), \quad (2)$$

and take $p_i = \exp(-\kappa^2/2)$ as the goodness of fit of the parameters for modelling the data at the grid point i . We thus build a probability distribution function (PDF) within the parameter grids by assigning p_i as the relative probability of the data to be modelled by the parameters at grid i . We project the PDF in the direction of each parameter, and find the contours that contain 99.5 per cent of the cumulative probability distribution. The half-width of these contours correspond to three times σ (error) of the parameter. The derived errors for the whole sample are listed in Table 1 (and displayed as a histogram in Fig. 2). We summarize our results as follows.

(i) r_s is well constrained ($\sigma < 1$ kpc) for most of the galaxies in the Bluedisk sample.

(ii) r_c often has large error bars ($\sigma > 2$ kpc), due to the resolution limit of the H I images.

Table 1. Parameters of the best-fitting models for the H I radial profiles.

ID	r_s (kpc)	σ_{r_s} (kpc)	r_c (kpc)	σ_{r_c} (kpc)	I_1 ($M_{\odot} \text{ pc}^{-2}$)	σ_{I_1} (dex)	I_2 ($M_{\odot} \text{ pc}^{-2}$)	σ_{I_2} (dex)
1	6.91	0.64	6.35	0.74	181.15	0.68	23.80	0.61
2	3.95	0.40	3.91	0.51	760.45	0.64	35.73	0.57
3	4.69	0.41	7.02	1.31	335.88	0.72	13.25	0.68
4	7.20	0.61	3.58	0.55	113.87	0.62	11.18	0.52
5	6.17	0.98	8.78	2.97	1162.44	0.69	79.04	0.65
6	7.83	0.60	6.32	0.40	310.51	0.80	45.73	0.77
8	7.84	0.74	5.79	0.75	64.62	0.67	9.94	0.55
9	3.62	0.38	3.28	0.73	1060.26	0.69	65.03	0.63
10	6.53	0.66	2.54	1.14	26.31	0.68	7.33	0.72
11	4.23	0.36	2.75	0.48	461.41	0.76	84.26	0.72
12	8.50	0.93	5.69	2.21	72.57	0.68	6.10	0.67
14	8.27	1.21	12.14	6.09	245.10	0.60	11.96	0.73
15	22.32	1.63	7.48	2.82	14.66	0.57	2.34	0.47
16	5.86	0.39	0.66	0.19	31.13	0.16	43.32	0.76
17	7.71	2.24	9.36	0.25	476.54	0.11	62.71	0.76
18	8.52	0.63	1.48	1.10	68.59	0.66	60.54	0.59
19	7.47	1.00	7.45	3.60	124.83	0.69	9.22	0.68
20	7.15	0.47	1.74	0.69	48.02	0.59	17.51	0.49
21	9.10	0.84	1.95	1.08	20.93	0.68	63.86	0.70
22	5.45	0.51	3.13	0.52	305.92	0.70	47.68	0.65
23	5.12	0.45	3.59	0.87	365.23	0.72	53.47	0.69
24	7.46	0.61	7.74	0.81	230.00	0.73	24.98	0.70
25	4.11	0.58	4.56	3.79	224.27	0.69	16.37	0.66
26	2.99	0.24	2.05	0.41	540.47	0.73	43.68	0.73
27	1.85	0.45	1.26	2.15	385.18	0.75	67.09	0.62
28	3.32	0.35	2.01	0.40	52.62	0.70	33.62	0.76
30	6.51	0.64	4.31	1.03	440.29	0.69	34.81	0.62
32	3.12	0.25	2.28	0.43	272.01	0.70	75.07	0.68
33	2.95	0.54	1.79	0.54	81.20	0.70	38.89	0.75
35	7.92	0.66	14.15	0.23	579.77	0.07	23.17	0.77
36	2.45	0.40	1.62	2.00	334.37	0.71	60.83	0.72
37	3.53	0.39	1.93	0.52	147.55	0.67	38.81	0.71
38	2.69	0.78	1.44	3.00	38.32	0.78	50.66	0.75
40	7.56	0.74	0.47	0.21	13.43	0.13	66.24	0.76
42	3.53	0.78	3.80	3.33	216.74	0.76	29.05	0.59
43	3.18	0.32	2.77	0.74	332.24	0.70	57.64	0.66
44	2.24	0.30	1.47	0.35	268.87	0.75	59.20	0.77
45	3.40	0.32	1.97	0.82	334.05	0.70	64.08	0.64
47	6.50	0.91	6.25	1.38	318.16	0.69	53.31	0.62
49	3.80	0.37	3.77	0.66	688.92	0.72	74.17	0.69
50	5.18	0.57	3.02	1.32	464.34	0.69	73.66	0.63

(iii) There is strong degeneracy between I_1 and I_2 for all the galaxies, the 1σ errors for both I_1 and I_2 are larger than 0.3 dex.

(iv) I_1/I_2 can be well constrained with $\sigma \sim 0.2$ dex for nearly half of the galaxies, but when the H I discs are relatively small ($R_1 < 30$ arcsec), I_1/I_2 cannot be robustly determined and has large errors.

We test our method with galaxies from the WHISP survey (Swaters et al. 2002) to ensure that our estimates of r_s will not be compromised by the resolution of Bluedisk H I images. We select the galaxies with optical images available from the SDSS and with stellar masses greater than $10^{9.8} M_{\odot}$. The publicly available total-intensity maps of the WHISP galaxies (with a median distance of $z \sim 0.008$) are rescaled in angular size so that they have similar dimensions to the Bluedisk galaxies (with median distance of $z \sim 0.026$), and convolved with a Gaussian point spread function (PSF) of 22×16 arcsec². We fit the model to the H I profiles from both the original WHISP images and the rescaled images. We compare these two estimates of r_s in Fig. 3. The two estimates correlate

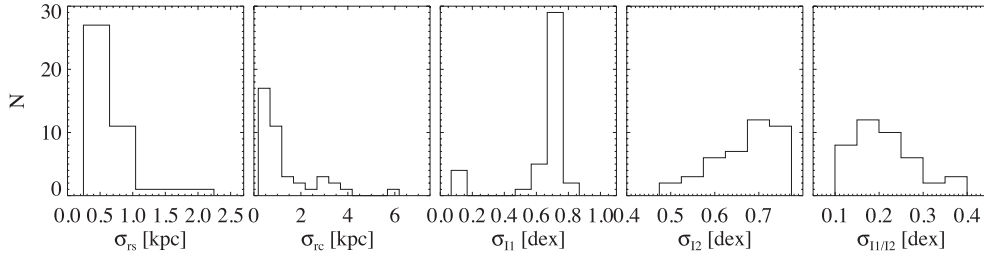


Figure 2. Distribution of errors on the parameters, r_s , r_c , I_1 , I_2 and I_1/I_2 in the best-fitting models for the H I radial profiles.

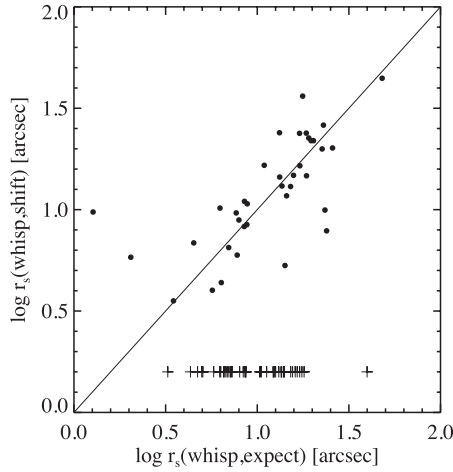


Figure 3. WHISP galaxies are shifted and convolved with the WSRT beam to have similar appearance to the BlueDisk galaxies. $r_s(\text{shift})$ are the scale-length measured from the shifted and convolved images, and $r_s(\text{expected})$ are the true scalelength expected at the redshifts of the BlueDisk galaxies. The crosses show the sizes of the BlueDisk galaxies.

with a correlation coefficient of 0.7 and there is no systematic offset. The scatter around the 1-to-1 line is 3.3 kpc, larger than the error listed in Table 1, because the WHISP data is much shallower than the BlueDisk data.

3.3 The universal H I RADIAL PROFILES IN OUTER DISCS

We divide the BlueDisk sample into three equal subsamples by their stellar properties (stellar mass, stellar mass surface density, colour, and colour gradient) and H I properties (H I: optical size ratio, H I mass fraction, H I mass, deviation from the C10 plane (see Section 2), and the morphological parameters ΔArea and ΔCenter). Instead of scaling the profiles by R25, the characteristic *optical* radius of the disc, we scale by R1, the radius where the column density of the H I is $1 M_\odot \text{pc}^{-2}$. The median H I radial profiles of the subsamples are displayed in Fig. 4. The outer H I profiles now display ‘Universal’ behaviour and exhibit an exponentially declining profile from ~ 0.75 to $1.3R_1$. Even the H I-rich galaxies (with large $\Delta f_{\text{H I}}$), which were postulated by C10 to have experienced recent gas accretion, the clumpy H I discs with large ΔArea , or H I disc that are off-centre with respect to the optical disc (with large ΔCenter), have outer H I profiles that do not deviate significantly.

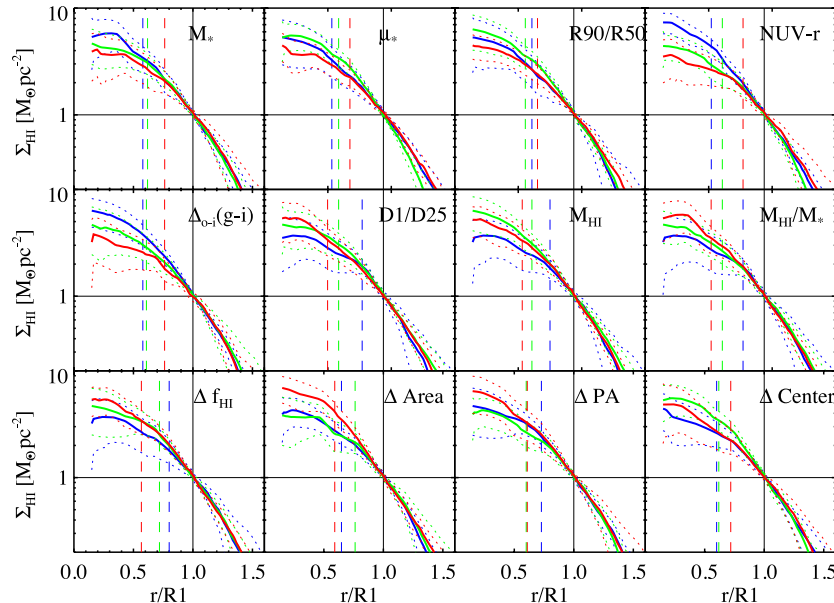


Figure 4. The galaxy sample is equally divided into three subsamples according to the parameter denoted at the top-right corner of each plot. These include stellar mass (M_*), stellar mass surface density (μ_*), concentration index (R90/R50), $NUV-r$ colour, colour gradient ($\Delta_{o-i}(g-i)$), H I-to-optical size ratio (D1/D25), H I mass ($M_{\text{H I}}$), H I mass fraction ($M_{\text{H I}}/M_*$), H I excess ($\Delta f_{\text{H I}}$), and H I morphological parameter ΔArea , ΔPA , and ΔCenter . The median H I profile for each subsample is plotted in blue for the lowest values of each parameter, in red for the highest values and in green for intermediate values. The dotted lines show the scatter around the median profiles. The dashed lines show the median value of R25/R1 for each of the subsamples. The solid lines indicate $R1 = 1$ and $\Sigma_{\text{H I}} = 1 M_\odot \text{pc}^{-2}$.

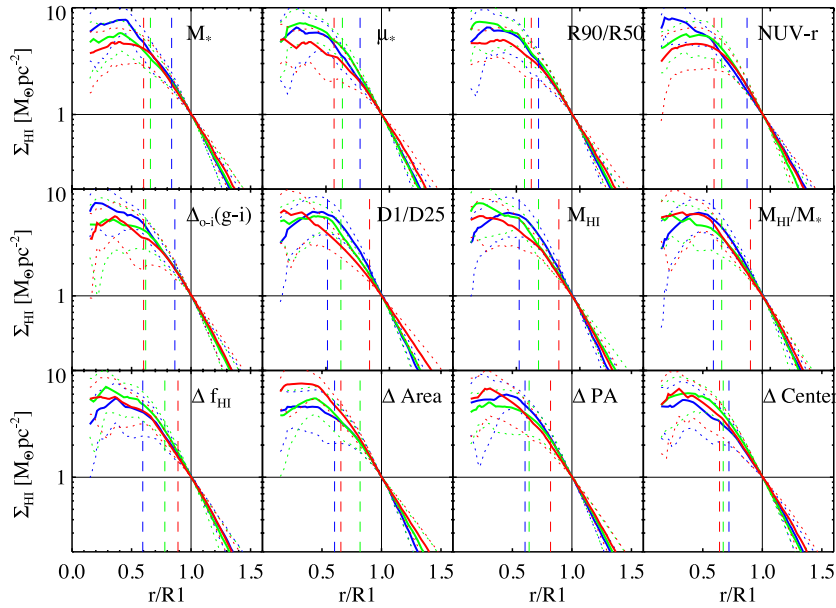


Figure 5. Similar as Fig. 4, but for the best-fitting model profiles.

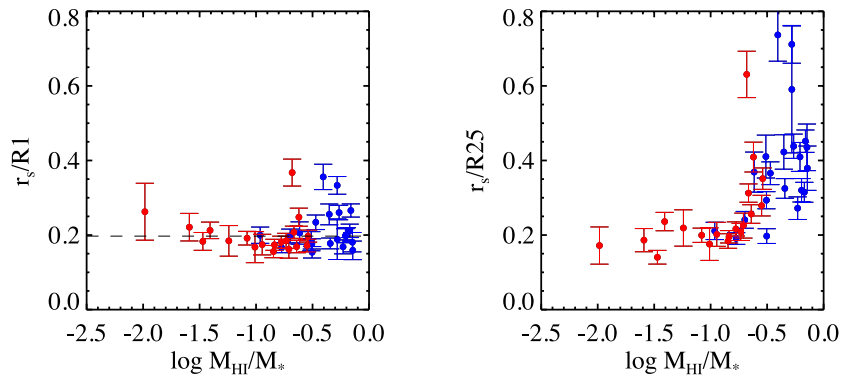


Figure 6. $r_s/R1$ (left) and $r_s/R25$ (right) are plotted as a function of H I mass fraction. The black dashed line shows the median value of $r_s/R1$. H I-rich galaxies are plotted in blue, while control galaxies are plotted in red.

We note that the median value of the averaged surface between 0.75 and 1.25 R1 is $\sim 1.142 \pm 0.022 M_\odot \text{pc}^{-2}$.

The differences between the inner profiles (at radii smaller than 0.75 R1) are much more prominent. They are most significant when the sample is split by $NUV - r$ colour, indicating a correlation with the SFRs.

In Fig. 5, we plot the best-fitting model profiles rather than the actual profiles. We can see that the homogeneous property in the outer profiles does not change. The fitted profiles show much steeper declines in the centre than the measured profiles, but we cannot make robust conclusions about it due to the resolution limit of the data. The median $\Sigma_{\text{HI},0.75-1.25\text{R1}}$ from the best-fitting models is $\sim 1.083 \pm 0.063 M_\odot \text{pc}^{-2}$. We plot the ratios $r_s/R1$ and $r_s/R25$ as a function of H I mass fraction in Fig. 6. From the left-hand panel, we can see that the dispersion of $r_s/R1$ around the median value of 0.19 ± 0.03 is small. There are two H I-rich galaxies (galaxy 15 and 21) and one control galaxy (galaxy 40) which deviate from the mean $r_s/R1$ by more than 0.1. These galaxies were not peculiar in terms of their H I mass (fractions), morphologies, global profiles, nor did their stellar properties differ in any clear way from the other galaxies in the sample.

From the right-hand panel of Fig. 6, we can see that $r_s/R25$ spans a much wider range of values, from 0.15 to 0.8, with most of the values below 0.6. The H I-rich galaxies have systematically higher H I-to-optical size ratios and also span a larger range in values.

The similarity of H I radial profile of different galaxies has been noticed before (e.g. Cayatte et al. 1994). Especially, a recent work by Martinsson et al. (2013, see also Martinsson 2011) pointed out that the half-maximum-radius of H I radial profiles of galaxies have a very narrow range if they are normalized by R1. Our work has gone further pointing out that the H I radial profiles of galaxies in the outer regions are homogeneous, by investigating the H I radial profiles in a large parameter space and by quantifying the exponential decline.

3.3.1 Relation to the H I mass–size relation

It is well known that in disc galaxies, the H I mass and the H I size R1 are tightly correlated (Broeils & Rhee 1997; Verheijen & Sancisi 2001; Swaters et al. 2002; Noordermeer et al. 2005; Paper I). Broeils

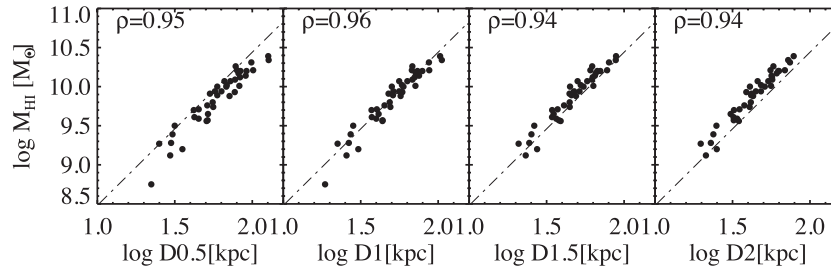


Figure 7. The relation between H I mass and the diameters of H I discs measured at a surface density of 0.5, 1, 1.5 and 2 $M_{\odot} \text{pc}^{-2}$. The correlation coefficient ρ is denoted in the corner of each figure. The dashed line shows the H I mass–D1 relation from Broeils & Rhee (1997).

& Rhee (1997) parametrize this relation as

$$\frac{M_{\text{HI}}}{M_{\odot}} = (12.88 \pm 3.85) \left[\frac{R1}{\text{pc}} \right]^2. \quad (3)$$

Our finding that the H I gas in the outer region of discs has a ‘universal’ exponential surface density profile offers a natural explanation for the tight H I mass–size relation. Our results also suggest that similar tight relations should be found for different definitions of H I size. This is illustrated in Fig. 7, where we show the correlations between M_{HI} and the radii where the H I surface density reaches 0.5, 1, 1.5 and 2 $M_{\odot} \text{pc}^{-2}$, respectively. As can be seen, the correlations are equally strong and tight for all four radii. The scatter in the H I mass–size relation only increases significantly at radii corresponding to surface densities greater than a few $M_{\odot} \text{pc}^{-2}$, where the total cold gas content is expected to be dominated by molecular rather than atomic gas.

3.3.2 Where is the ‘excess’ H I gas located?

In this section, we subtract the median H I profile of galaxies in the ‘control’ sample from the H I profile of each H I-rich galaxy, in order to study the spatial distribution of the excess gas. Results are shown in Fig. 8. Interestingly, there appear to be one class of galaxy (e.g. 2,3, 16, 14, 4, 18, 20, 5, 19) where the excess rises monotonically towards the smallest radii, or peaks well within the optical radius R25. In a second class of galaxy (e.g. 22, 35, 47, 24, 1, 12, 15, 6, 30, 8, 17), the excess peaks very close to R25 and drops off on either side. The latter class of excess gas is still found when we apply the analysis to the total cold gas profiles (which are derived in Section 4), so is not likely to be connected with the atomic-to-molecular gas conversion, but is suggestive of recent accretion of a ring of gas at the edge of the optical disc.

4 THE TOTAL COLD GAS PROFILES

B12 analysed average gas radial distributions of 17 star-forming massive disc galaxies. They found that if they re-normalized the surface densities by dividing by the transition surface density Σ_{transit} where Σ_{H_2} equals Σ_{H_1} , and dividing the radii by R25, the characteristic optical radius of the disc, the resulting gas radial profiles exhibited a ‘Universal’ exponential distribution beyond 0.2 R25, which could be parametrized as

$$\Sigma_{\text{gas}} / \Sigma_{\text{transit}} = 2.1e^{-1.65r/R25}. \quad (4)$$

In this section we explain how we construct total cold gas radial profiles for our Bluedisk galaxies, for comparison with the B12 results. We do not have information about the molecular gas in all the Bluedisk galaxies, and the spatial resolution of the Bluedisk

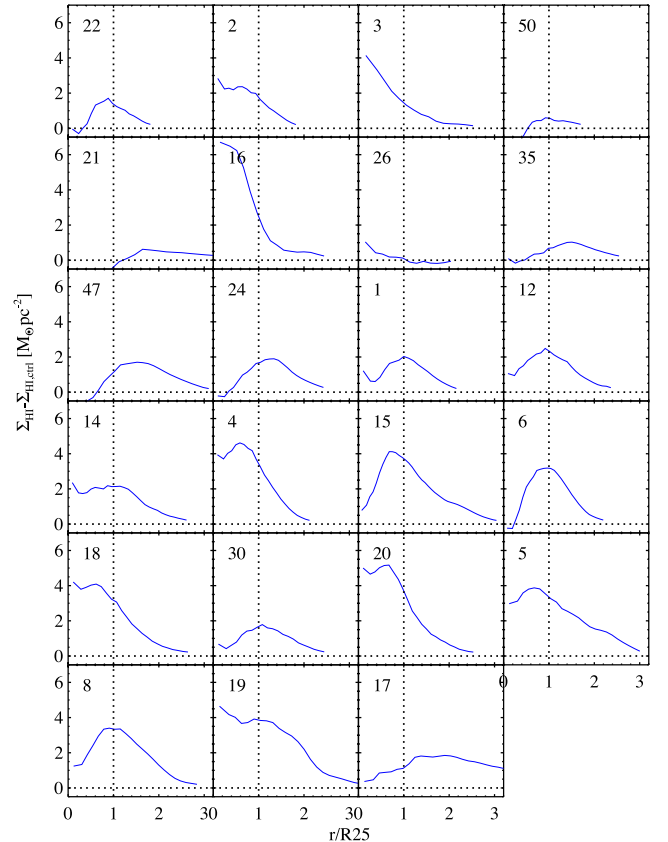


Figure 8. The difference between the H I profiles for the H I-rich galaxies and the median H I profile of the control galaxies. The dashed lines show where the radius equals R25. The IDs of the H I-rich galaxies are denoted in the corner of each panel.

H I data (FWHM of PSF ~ 10.6 kpc) is lower than the B12 data (FWHM of PSF ~ 1 kpc).

First, we use the SFR radial profiles to provide an estimate of the H_2 radial profiles for our galaxies. We use the *GALEX* far-ultraviolet (FUV) images and the *WISE* 22 μm images to derive the SFR profiles (Σ_{SFR}). The FUV images were converted to the resolution of the 22 μm images. Following Wright et al. (2010) and Jarrett et al. (2011), we apply a colour correction to the 22 μm luminosity of extremely red sources. We calculate the IR-contribution to the star formation rate (SFR_{IR}) of our sample by adopting the relation between SFR and *WISE* 22 μm luminosity in Jarrett et al. (2013). We adopt the formula from Salim et al. (2007) to derive the UV contribution to the star formation rate, SFR_{FUV} . The final SFR is the sum of SFR_{IR} and SFR_{FUV} . Σ_{SFR} is then converted into an estimated

H₂ surface density using the formula in Bigiel et al. (2008). The total gas radial profile is calculated as

$$\Sigma_{\text{gas}} = 1.36 (\Sigma'_{\text{H}_2} + \Sigma_{\text{H}_1}), \quad (5)$$

where the factor of 1.36 corrects for the contribution from helium.

To confirm that this technique is robust, we apply it to the subsample of galaxies from the WHISP survey, which have *GALEX* near-ultraviolet (NUV) and *WISE* 22 μm images. Following the sample definition in B12, we select massive ($M_*/M_\odot > 10^{9.8}$), relatively face-on (size ratio $b/a > 0.5$, or inclination angle smaller than 60°) star-forming ($\text{NUV} - r < 3.5$) disc (concentration $R90/R50 < 2.8$) galaxies. The *WISE* 22 μm images have similar resolution to the B12 images. The H I images of the WHISP galaxies have a FWHM PSF of ~ 2 kpc, again very similar to that of the B12 images. The black points in the top panel of Fig. 9 show the average, scaled cold gas radial surface density profile. The relation derived by B12 is shown in orange, and the agreement is very good.

Following B12, to minimize resolution effects, the analysis is performed on the relatively face-on ($b/a > 0.5$) Bluedisk galaxies, which include 12 H I-rich galaxies and 14 control galaxies. We note that the H I maps of the Bluedisk galaxies have considerably worse resolution (FWHM of PSF ~ 10 kpc) than the B12 gas maps. We use the best-fitting model H I profiles derived in the last section, instead of the directly measured H I radial profiles. Because Σ_{transit} varies little from galaxy to galaxy, we assume a fixed $\Sigma_{\text{transit}} \sim 14 M_\odot \text{pc}^{-2}$ from the B12 relation (Leroy et al. 2008) rather than calculating Σ_{transit} from the best-fitting model H I profile. This is because the fit in the inner region has large uncertainties (Section 3.2). Our results are shown in the middle and bottom panels of Fig. 9. From the middle panel of Fig. 9, we see that within 2R25 the mean gas profile of the Bluedisk sample is also consistent with the B12 relation. The individual profiles exhibit a large scatter around the B12 relation in the outer regions (beyond R25). In the bottom panel of Fig. 9, we plot the mean gas profile of the control galaxies in red and the mean profile of the H I-rich galaxies in blue. The mean profile of the H I-rich galaxies lies slightly above the B12 relation, while that of the control galaxies lies significantly below the B12 relation. This is consistent with our previous findings (Paper I) that H I-rich galaxies have larger R1/R25 than the control galaxies.

To summarize, the radial gas profile of Bluedisk galaxies exhibit large scatter around the B12 relation in their outer regions. The control galaxies deviate significantly from the B12 relation, which may be connected with the low accretion rate of cold gas or more evolved H I discs.

5 COMPARISON WITH SPH SIMULATIONS AND SEMI-ANALYTIC MODELS

In this section, we will compare the results presented in the previous sections with the SPH simulations of Aumer et al. (2013) and the semi-analytic models of Fu et al. (2013).

5.1 Comparison with SPH simulations

We compare our observed H I profiles to those found in 19 $z = 0$ galaxies from cosmological zoom-in SPH simulations. The simulations were described in detail in Aumer & White (2013), Aumer et al. (2013) and follow the formation of galaxies in haloes with masses $1 \times 10^{11} < M_{200}/M_\odot < 3 \times 10^{12}$ in a Λ cold dark matter (Λ CDM) universe. The simulations include models for multiphase gas treatment, star formation, metal enrichment, metal-line cooling, turbulent metal diffusion, thermal and kinetic supernova feedback

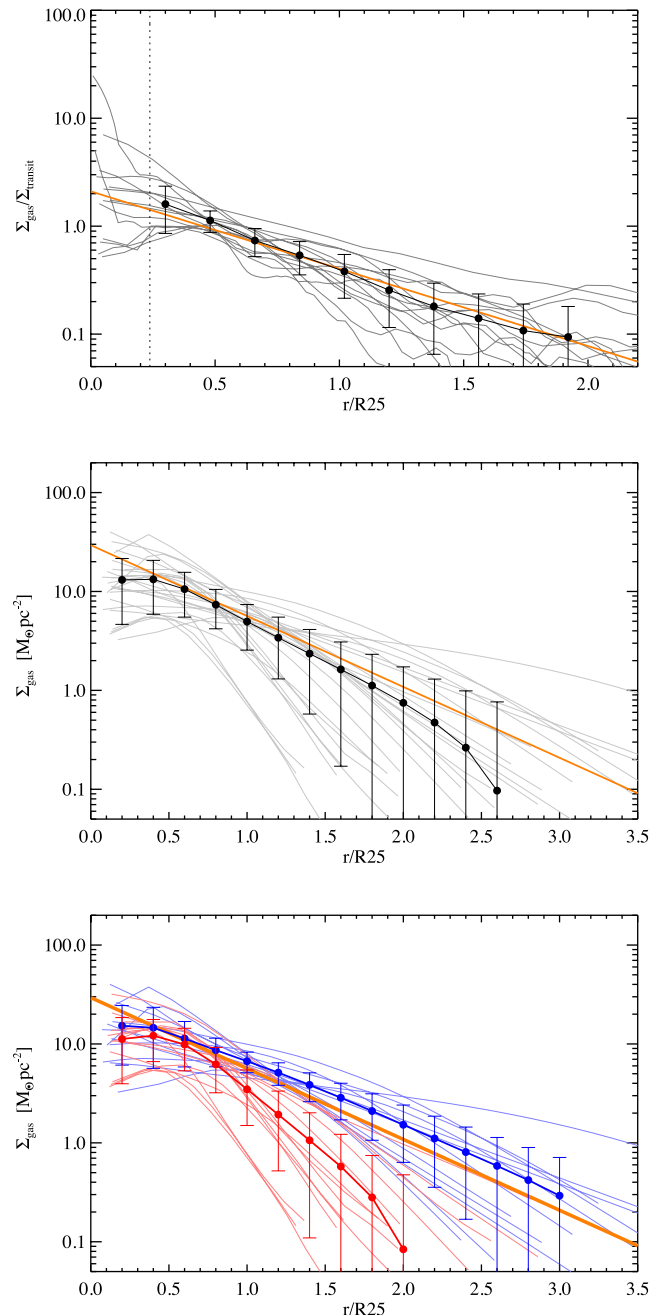


Figure 9. Top panel: estimated total gas profiles for the WHISP galaxies (grey). The black points show the average profile and the error bars indicate the 1σ scatter derived from bootstrapping. The orange line shows the universal relation obtained by B12 when interacting systems are excluded. Middle panel: similar to the top panel, but for the Bluedisk galaxies. A fixed transition surface density $\Sigma_{\text{transit}} \sim 14 M_\odot \text{pc}^{-2}$ is assumed (Leroy et al. 2008). Bottom panel: the same as the middle panel, except that the red lines are for the control galaxies and the blue lines are for the H I-rich galaxies.

and radiation pressure from young stars. They lack, however, a model for the partition of atomic and molecular gas in interstellar medium.

As was shown in Aumer & White (2013), the $z = 0$ model galaxies all contain gas discs, with gas fractions that are higher than the observed average at the same stellar mass. The model disc galaxies are thus quite comparable in H I content to the Bluedisk galaxies. To obtain H I profiles for the simulated discs, we apply

a simple model based on the observationally motivated model by Blitz & Rosolowsky (2006). The same model was used in the semi-analytic models of Fu et al. (2010).

We first select all gas with $T < 15000$ K and determine its angular momentum vector to orient the galaxy in a face-on orientation. We then divide the galaxies into quadratic pixels with 500 pc side length. According to Blitz & Rosolowsky (2006) the ratio of molecular and atomic hydrogen is

$$f_{\text{mol}}(x, y) = \Sigma_{\text{H}_2}(x, y) / \Sigma_{\text{H I}}(x, y) = (P(x, y) / P_0)^\alpha, \quad (6)$$

where $\alpha = 0.92$ and $P_0 = 5.93 \times 10^{-13}$ Pa are constants fit to observations. For the mid-plane pressure $P(x, y)$ we use the relation given by Elmegreen (1993),

$$P(x, y) = \frac{\pi}{2} G \left[\Sigma_{\text{gas}}(x, y)^2 + f_\sigma(x, y) \Sigma_{\text{gas}}(x, y) \Sigma_{\text{stars}}(x, y) \right], \quad (7)$$

with the ratio of gas-to-stellar velocity dispersions

$$f_\sigma(x, y) = \frac{\sigma_{\text{gas}}(x, y)}{\sigma_{\text{stars}}(x, y)}, \quad (8)$$

which, as the surface densities, we take directly from the simulations. To account for ionized hydrogen among the $T < 15000$ K gas, we assume a 25 percent ionized fraction in stellar dominated regions and correct for the absence of stars as a source of ionization by crudely invoking a factor $\Sigma_{\text{gas}} / \Sigma_{\text{stars}}$ where stars are subdominant.

The resulting H I surface density $\Sigma_{\text{H I}}(x, y)$ is then used to create face-on H I profiles $\Sigma_{\text{H I}}(r)$ for all model galaxies. R1 is then determined as the radius, where $\Sigma_{\text{H I}}(r)$ drops below $1 M_\odot \text{ pc}^{-2}$ and the H I mass $M_{\text{H I}}$ as the total mass out to the radius, where $\Sigma_{\text{H I}}(r)$ drops below $0.2 M_\odot \text{ pc}^{-2}$, which corresponds to the detection threshold of the Bluedisk sample. To consider the effect of beam smearing in observations, we convolve $\Sigma_{\text{H I}}(x, y)$ with an elliptical Gaussian Kernel with FWHM values of 14 and 9 kpc for major and minor axes. From the convolved surface density $\Sigma_{\text{H I, smooth}}(x, y)$, we then derive $\Sigma_{\text{H I, smooth}}(r)$, $M_{\text{H I, smooth}}$ and $\text{R1}_{\text{smooth}}$.

5.1.1 Results of the SPH simulation

The results of a comparison between simulations and observations are depicted in Fig. 10.

In the upper-left panel we depict the H I-to-stellar mass ratio $M_{\text{H I}} / M_{\text{stars}}$ as a function of stellar mass M_{stars} for the simulated and observed galaxies. The simulations (red) span a wider range in stellar mass ($9.5 < \log(M_{\text{stars}} / M_\odot) < 11.3$) than the observations which were limited to $10. < \log(M_{\text{stars}} / M_\odot) < 11$. In terms of gas richness, by construction about half of the observed galaxies lie above the black dashed line which depicts the median relation found by C10 (solid black line) shifted up by 0.6 dex. Only 4 of 19 simulated galaxies are above this line. The remaining simulated galaxies have a similar distribution of H I-mass fraction as the control sample, which have lower gas fractions.

In the upper-right panel of Fig. 10 we depict the H I mass–size relation. For the observed galaxies, we use D1 values corrected for beam-smearing effects and for simulated galaxies, we use unconvolved values. We see that the observed and the simulated samples both follow the relation found by Broeils & Rhee (1997). The agreement between the simulations and the observations is very good. The simulations show a very mild offset to lower H I masses, which may be connected to the difference in gas fraction of the samples or a minor problem of the H I modelling. Note also that the

range of sizes of the galaxies in the two samples is very similar. We find that the largest H I discs in simulations form from gas that cools and settles in a disc after merger events at $z \sim 1$.

In the lower-left panel of Fig. 10 we depict a compilation of all 19 beam-convolved simulated H I-mass profiles $\Sigma_{\text{H I, smooth}}(R)$ with radius R in units of R1. All profiles have similar shape. They are rather flat in the centre and fall exponentially at $R > 0.75$ R1. The central values in surface density scatter between 2 and $5 M_\odot \text{ pc}^{-2}$, the outer exponential scalelengths are between 0.15 and 0.45 R1. We overplot the simulated median profile (red line) and the observed median profile of the Bluedisk galaxies (blue diamonds). We note that there is good agreement between simulations and observations. The central surface densities in simulations are slightly lower than in observations, consistent with the slightly lower H I masses shown in the top-left panel. The outer profile at $R > 0.5$ R1 agrees very well with the observations.

The dashed purple and black curves show the median profiles we obtain, when we use the offset of the H I-to-stellar mass ratio of the simulated galaxies from the solid black line in the upper-left panel of Fig. 10 to equally divide the simulated sample into a gas-rich (purple) and a gas-poor (black) subsample. We find that the gas-rich sample has higher central surface densities and shows steeper decline at outer radii compared to the gas-poor sample. This differs from the observation that gas richness has no influence on the outer slope. We caution however that we are looking at two samples with ~ 10 objects each. Considering the corresponding statistical errors, there is no significant disagreement between the outer slopes. Moreover, if we use means instead of medians, the difference in outer scalelength becomes very small.

Finally, we show the outer disc exponential scalelength r_s in units of R1 as a function of H I mass $M_{\text{H I}}$ in the lower-right panel. We fit exponentials to the outer regions ($R > 0.8$ R1) of the raw, unconvolved H I mass profiles from the simulations and compare the corresponding r_s values (red stars) to observational values corrected for beam effects (blue diamonds). Not all simulated outer profiles are well fitted by exponentials. For a few cases, where there is a significant flattening visible for the very outer gas disc, we restrict the exponential fit to the region around $R = \text{R1}$.

We find that the median (un-convolved) outer H I scalelength is 0.175 in units of R1, which compares well to the median beam-corrected value of 0.19 found for the Bluedisk sample. The longest scalelength in the observations (~ 0.45) is connected to a galaxy–galaxy interaction. The main difference between simulations and observations is found for the lowest r_s values, which are limited to ~ 0.15 for the Bluedisk galaxies, but extend to ~ 0.10 for the simulated galaxies. We note that for the simulated profiles the scatter of r_s values is reduced by the application of the beam correction. As shown in the lower-left panel, the resulting profiles agree well with the median observed profile.

5.2 Comparison with semi-analytic models

In this section, we compare the observations with the semi-analytic models of galaxy formation of Fu et al. (2013; hereafter Fu13). In these models, each galaxy disc is divided into a series of concentric rings to trace the radial profiles of stars, interstellar gas and metals. Physical prescriptions are adopted to partition the interstellar cold gas into atomic and molecular phases. In order to take into account the effects of beam smearing in the observations, the model radial profiles of $\Sigma_{\text{H I}}$ are convolved by a Gaussian function with $\text{FWHM} = 10.6$ kpc. The radius R1 is then derived from these smoothed profiles. In order to carry out as fair a

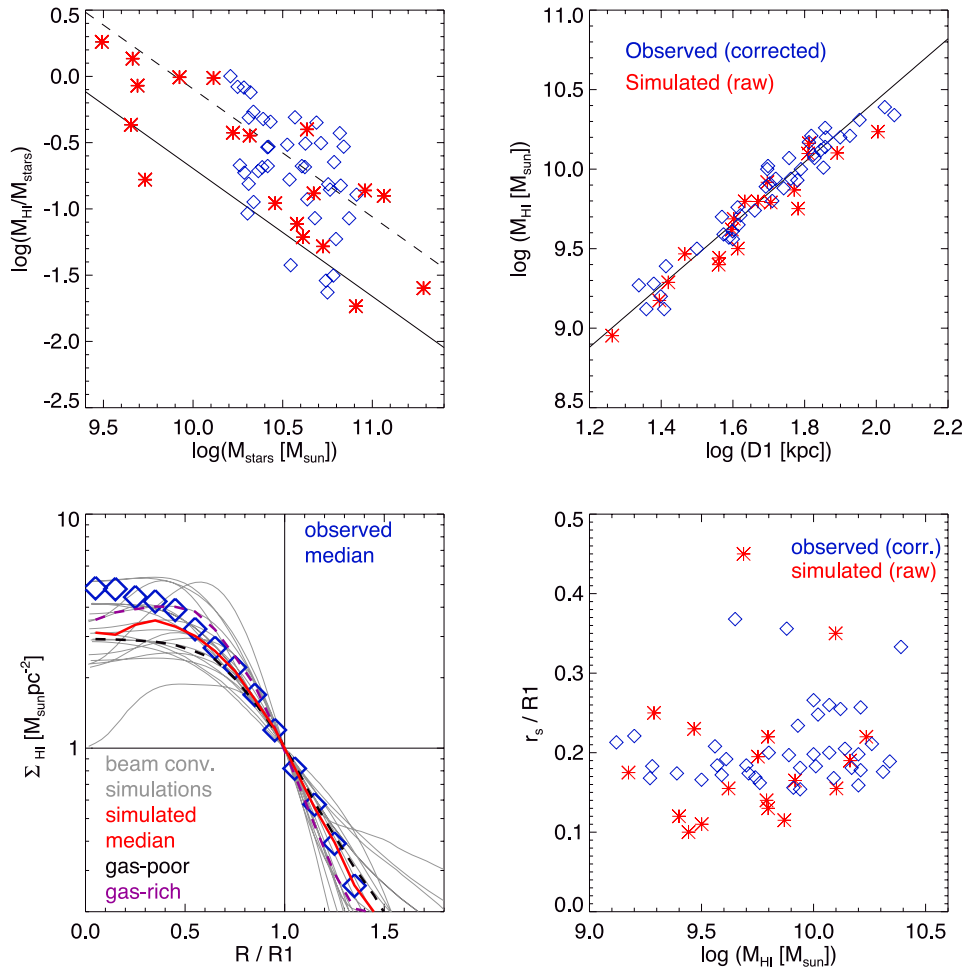


Figure 10. A comparison of the SPH simulations and the BlueDisk observations. Panel 1: the H I-to-stellar mass ratio $M_{\text{HI}}/M_{\text{stars}}$ as a function of stellar mass M_{stars} for simulated (red stars) and observed galaxies (blue diamonds). The solid black line shows the median relation between H I mass fraction and stellar mass found by C10, the dashed black line is offset from this relation by +0.6 dex. Panel 2: the H I mass–size relation. For simulations (red stars) we plot M_{HI} and $D1 = 2 R1$ determined from the un-convolved profiles, for observations (blue diamonds) we plot values that were corrected to account for beam effects. Overplotted in black is the relation found by Broeils & Rhee (1997). Panel 3: H I mass profiles for radii normalized to R1. In light grey, we plot the convolved profiles $\Sigma_{\text{HI,smooth}}(r)$ for all 19 simulated discs. We overplot the simulated median profile (red line) and the observed median profile (blue diamonds). We also show the medians for a gas-rich (purple dashed) and a gas-poor (black dashed) subsample. Panel 4: the relation between $r_s/R1$ and H I mass. We show values for the un-convolved, raw profiles from the simulations (red stars) and for observational values which were corrected to account for beam effects (blue diamonds).

comparison with the observations as possible, we select the galaxy with $\log_{10}[M_{\text{HI}}/M_{\odot}] > 9.0$, $10.0 < \log_{10}[M_{\text{HI}}/M_{\odot}] < 11.0$ and $-1.8 < \log_{10}[M_{*}/M_{\text{HI}}] < 0.2$ from the model sample at $z = 0$.

5.2.1 Results from the semi-analytical model comparison

In the top two panels of Fig. 11, we show the H I-to-stellar mass ratio as a function of stellar mass for the Fu13 model galaxies and the BlueDisk sample. The two panels represent the model results with two H_2 fraction prescriptions. The blue points correspond to individual model galaxies, while the red points correspond to individual BlueDisk galaxies. The grey shaded area shows the 1σ deviation around the median relation between M_{HI}/M_{*} and M_{*} for the model galaxies. By construction, the model galaxies span the same range in stellar mass and H I mass fraction as the BlueDisk sample. In the middle two panels of Fig. 11, we show the H I mass–size relation for the models and the data. The R1 values from the observations are corrected for beam smearing and the model values are un-convolved. The model results fit both the Broeils & Rhee

(1997) and the observational data extremely well. The tight correlation between H I size and mass is a result of the conversion between H I and H_2 in the model. Too high H I column density makes H I atom form H_2 , and the average column density of H I-rich galaxies does not drop below several $M_{\odot} \text{pc}^{-2}$. Thus, the H I-rich galaxies always have a narrow distribution of average surface density. Finally, the bottom two panels show the relation between $r_s/R1$ and H I mass for both models and data. r_s is defined as the scalelength of the H I profile at $r > 0.75R1$ obtained by fitting an exponential profile to this region of the disc. The black solid curves show the model median values and the error bars represent the $\pm 1\sigma$ deviations around the median. $r_s/R1$ is around 0.22 to 0.24 for model galaxies, compared to 0.19 for the BlueDisk sample.

Finally, in Fig. 12, we show the beam-convolved H I radial surface density profiles in units of $r/R1$ from the Fu13 models with two H_2 fraction prescriptions. Similar to Fig. 4, we divide model samples into three equal parts according to stellar mass M_{*} , H I mass M_{HI} , and H I-to-stellar mass ratio M_{HI}/M_{*} , from the top to bottom rows. In each panel, the red, green and blue curves represent the median

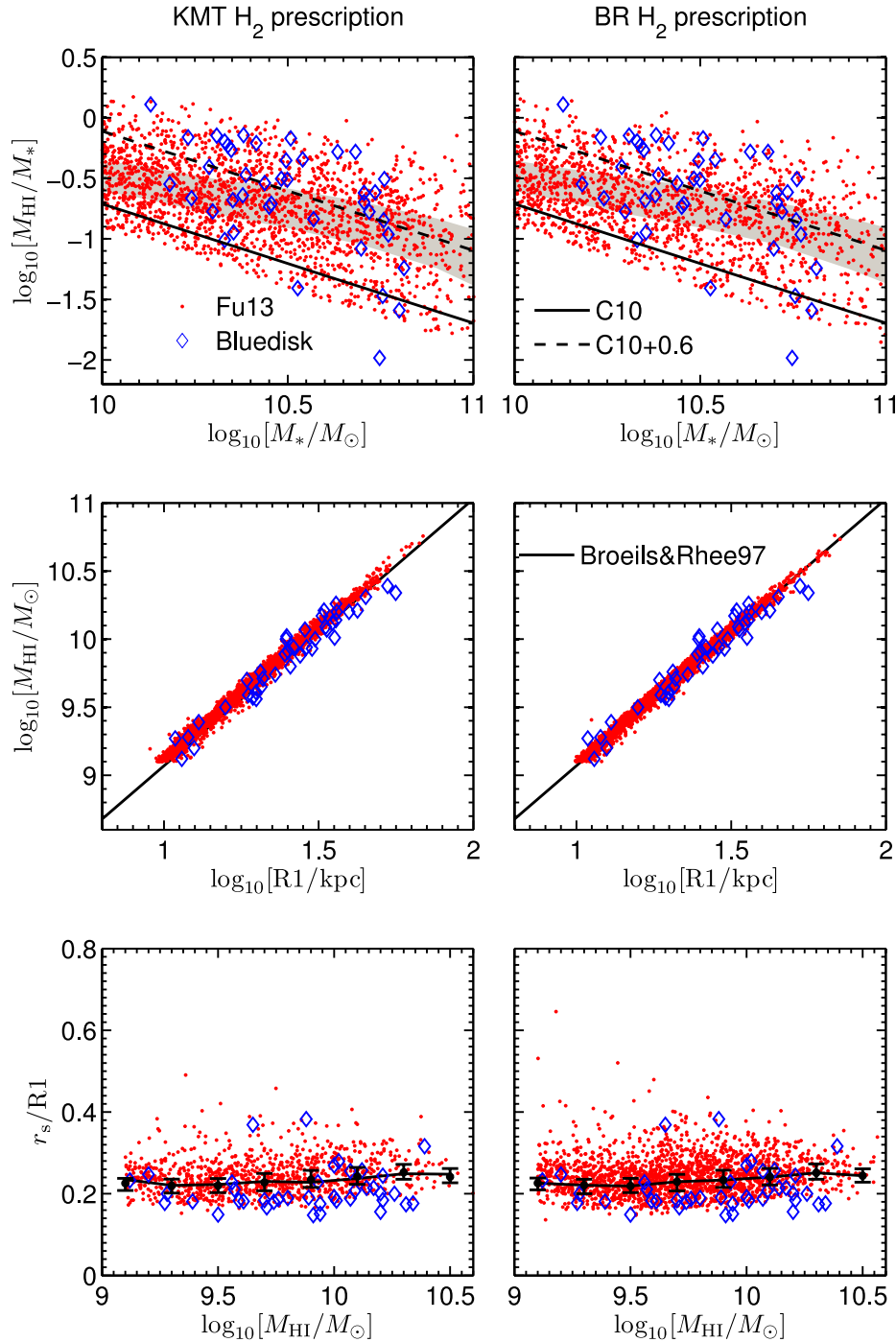


Figure 11. The comparison between the Fu13 model results and the Bluedisk observational sample. The two columns represent the Fu13 models with two H₂ fraction prescriptions (see Fu13 for details). In each panel, the red dots represent the model sample and the blue dots are for the Bluedisk sample. Top two panels: the H_I-to-stellar mass ratio as a function of stellar mass. The grey areas represent the $\pm 1\sigma$ deviations around the mean values for the Fu13 model sample. For comparison, the black solid lines show the median relation in C10 and black dashed lines are offsets from solid lines by 0.6 dex. Middle two panels: The H_I mass–size relation. The R1 values from observations are corrected for beam-smearing effects and R1 values from models are un-convolved. The black lines represent the fitting equation in Broeils & Rhee (1997, the diameter D1 is converted to radius R1). Bottom two panels: the relation between $r_s/R1$ and H_I mass. The black solid curves represent the model median values and the error bars represent the $\pm 1\sigma$ deviations around the median values for the model sample. $r_s/R1$ values from models are un-convolved and $r_s/R1$ values from Bluedisk observations are beam-corrected values.

model profiles for the highest, intermediate, and lowest values of each parameter. The black curves show the median profile of the Bluedisk sample.

As can be seen, the model and the observational profiles agree extremely well in the outer disc. The H_I density profiles in the

inner disc are systematically too high compared to observations. When the sample is split according to H_I mass or H_I mass fraction, the same *qualitative* trends are seen in both models and data. We will explain the origin of these trends in the next section.

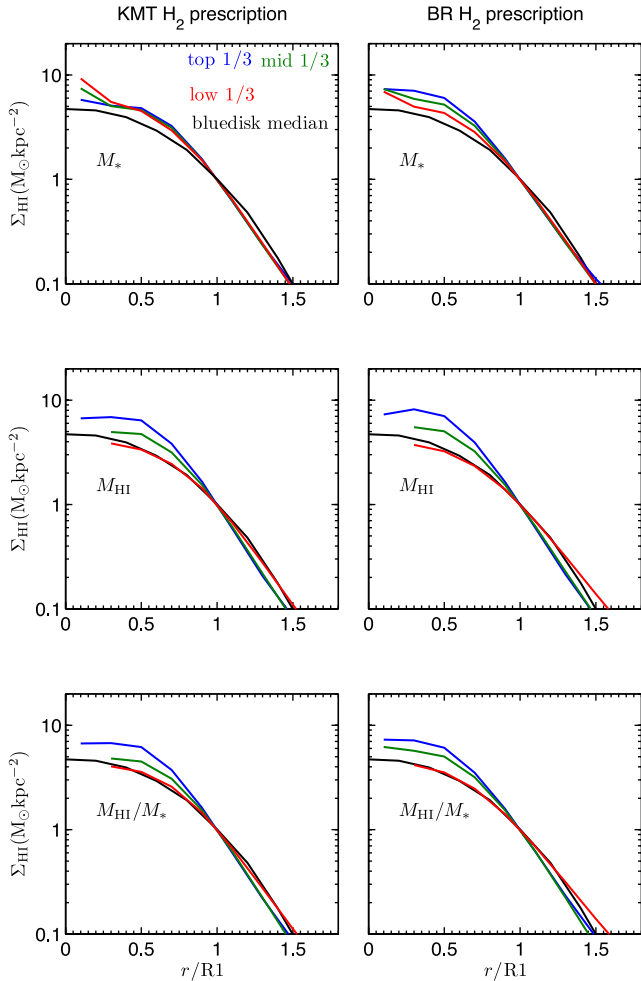


Figure 12. The relation between beam-convolved H I radial surface density profiles Σ_{HI} and the normalized radius $r/R1$ from the [Fu13](#) model. The two columns represent the results of models with two H_2 fraction prescriptions. Similar to Fig. 4, the model samples are equally divided into three parts by M_* , M_{HI} and M_{HI}/M_* from the top to bottom rows. In each panel, the red, green and blue curves represent the median profiles in the lowest to highest parameter bins. The black curves represent the median curves from the whole Bluedisk sample.

6 INTERPRETATION OF THE HOMOGENEOUS OUTER H I PROFILES

6.1 Outer H I PROFILES IN SEMI-ANALYTIC MODELS

We have demonstrated that the outer disc H I surface density profiles have universal form when scaled to a radius corresponding to a fixed H I surface density and that the slope of the outer disc $r_s/R1$ is almost constant among different galaxies.

In the [Fu13](#) models, newly infalling gas is assumed to be distributed exponentially and is directly superposed on to the pre-existing gas profile from the previous time step. Gas also flows towards the centre of the disc with inflow velocity $v_{\text{inflow}} = \alpha r$ ($v_{\text{inflow}} \sim 7 \text{ km s}^{-1}$ at a galactocentric radius of 10 kpc). Following the prescription in [Mo, Mao & White \(1998\)](#), the scalelength of the exponential infalling gas is given by $r_{\text{cool}} = (\lambda/\sqrt{2})r_{\text{vir}}$, in which λ and r_{vir} are the spin parameter and virial radius of the galaxy’s dark matter halo. Since the increase of r_{vir} and r_{cool} scales with the age of the Universe, the outer disc gas profiles are mainly deter-

mined by recent gas accretion. This disc galaxy growth paradigm is called ‘inside-out’ disc formation (e.g. [Kauffmann 1996](#); [Dutton et al. 2007](#); [Fu et al. 2009](#)), and an illustration of inside-out growth of the gas disc can be found in fig. 1 in [Fu et al. \(2010\)](#).

According to the definition of outer disc scalelength r_s , the outer disc H I surface density profile can be written as

$$\Sigma_{\text{HI}} = \Sigma_0 \exp\left(-\frac{r}{r_s}\right) \quad (9)$$

in which Σ_0 is disc central H I surface density extrapolated from the outer disc H I profile. Let us suppose that r_s in equation (9) is approximately equal to r_{infall} at the present day, and Σ_0 represents the amount of gas accreted at $r = 0$ in the recent epoch.

Substituting $1 \text{ M}_\odot \text{ pc}^{-2} = \Sigma_0 \exp(-R1/r_s)$ into equation (9), $r_s/R1$ can be written as

$$\frac{r_s}{R1} = \frac{1}{\ln[\Sigma_0/\text{M}_\odot \text{ pc}^{-2}]} \quad (10)$$

Equation (10) implies that $r_s/R1$ actually relates to the amount of recent gas accretion at $r = 0$. For simplicity, we define $\dot{\Sigma}_0 = d\Sigma_0/dt$ as the cold gas infalling rate at $r = 0$.

We have tested the correlation between $r_s/R1$ and $\dot{\Sigma}_0$ averaged over different time-scales. We find the best correlation with $r_s/R1$ if $\dot{\Sigma}_0$ is averaged over a time-scale corresponding to the past 0.5 Gyr. In the left-hand panel of Fig. 13, we plot the relation between $r_s/R1$ and $1/\ln \dot{\Sigma}_0$ (averaged in the recent 0.5 Gyr) for model galaxies with $M_* > 10^{10} \text{ M}_\odot$ and $M_{\text{HI}} > 10^9 \text{ M}_\odot$, based on KMT H_2 prescription. The blue solid line represents the fitting equation

$$r_s/R1 = 0.065 + (\ln[\dot{\Sigma}_0/\text{M}_\odot \text{ pc}^{-2} \text{ Gyr}^{-1}])^{-1}. \quad (11)$$

However, we note that a correlation between $r_s/R1$ and H I excess (Δf_{HI}) is not found from the observation (Section 3.3).

The right-hand panel of Fig. 13 shows the relation between M_{HI} and $\dot{\Sigma}_0$. There is no relation between the two quantities, i.e. H I mass alone cannot be used to infer the recent accretion rate of a galaxy.

To summarize: the universal outer disc profiles in the semi-analytic models originate from the combination of the *assumption* that infalling gas has an exponential profile and of the inside-out growth of discs.

6.2 Main caveats

We note that the assumption that gas accreted from the halo is distributed on the disc with an exponential profile has no a priori physical justification. [Bullock et al. \(2001\)](#) studied the angular momentum profiles of a statistical sample of haloes drawn from high-resolution N -body simulations of the Λ CDM cosmology and showed that the cumulative mass distribution of specific angular momentum j in haloes could be fitted with a function that follows a power law and then flattens at large j .

They explored implications of their $M(<j)$ profile on the formation of galactic discs assuming that j is conserved during infall. They showed that the implied gas density profile deviates from an exponential disc, with higher densities at small radii and a tail extending to large radii.

It is thus something of mystery why the hydrodynamical simulations presented in this paper have outer discs that agree so well with the observed ‘universal’ outer exponential profiles seen in the data. The solution likely lies in the complicated interplay between the infall of new gas, star formation, supernova feedback and gas inflow processes occurring in the simulation and will form the subject of future work.

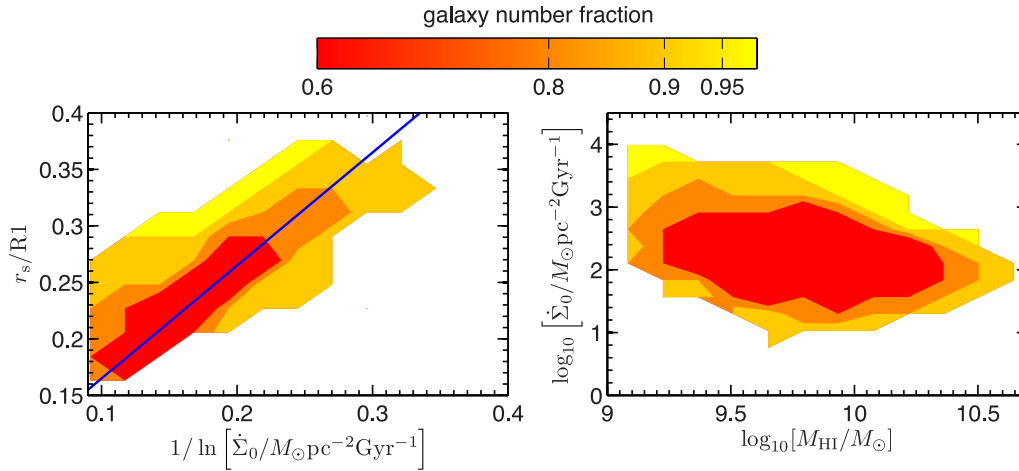


Figure 13. Left-hand panel: the relation between $r_s/R1$ and $1/\ln[\dot{\Sigma}_0/M_\odot \text{pc}^{-2} \text{Gyr}^{-1}]$ for model galaxies. $\dot{\Sigma}_0$ is the gas infall rate in the disc centre averaged over the past 0.5 Gyr and r_s is the exponential scalelength of the outer disc. The blue solid line is the fitting line equation (11). Right-hand panel: the relation between $\dot{\Sigma}_0$ and M_{HI} for model galaxies. In both panels, the galaxies are from model results with KMT H_2 fraction prescription at $z = 0$. The contours indicate the fraction of model galaxies located in a given region of parameter space, as given by the colour key at the top of the plot.

7 SUMMARY

We have measured the azimuthally averaged radial profiles of H I gas in 42 galaxies from the Bluedisc sample. We investigated how the shape of H I profiles vary as a function of galactic properties. We developed a model to describe the shape of H I profiles which is an exponential function of radius in the outer regions and has a depression towards the centre. We derive maximum-likelihood estimates of r_s , the scale radius of the outer exponential H I disc. By inverting the relation between SFR and H_2 surface density, we also derive estimates of the total gas surface density profiles of our galaxies. Finally, we compare our observational results with predictions from SPH simulations and semi-analytic models of galaxy formation in a ΛCDM universe. The main results can be summarized as follows.

(i) The H I discs of galaxies exhibit a homogeneous radial distribution of H I in their outer regions, when the radius is scaled to $R1$, the radius where the column density of the H I is $1 M_\odot \text{pc}^{-2}$. The outer distribution of H I is well fitted by an exponential function with a scalelength of $0.18 R1$. This function does not depend on stellar mass, stellar mass surface density, optical concentration index, global $\text{NUV} - r$ colour, colour gradient, H I mass, H I -to-stellar mass fraction, H I excess parameter, or H I disc morphologies.

(ii) By comparing the radial profiles of the H I -rich galaxies with those of the control systems, we deduce that in about half the galaxies, most of the excess gas lies outside the stellar disc, in the exponentially declining outer regions of the H I disc. In the other half, the excess is more centrally peaked.

(iii) The median total cold gas profile of the galaxies in our sample agrees well with the ‘universal’ radial profile proposed by B12. However, there is considerable scatter around the B12 parametrization, particularly in the outer regions of the disc.

(iv) Both the SPH simulations and semi-analytical models are able to reproduce the homogeneous profile of H I in the outer region with the correct scalelength. In the semi-analytic models, the universal shape of the outer H I radial profiles is a consequence of the *assumption* that infalling gas is always distributed exponentially.

ACKNOWLEDGEMENTS

We gratefully thank T. Oosterloo, M. A. W. Verheijen, R. Yates and L. Shao for useful discussions. We thank the anonymous referee for constructive comments.

Galaxy Evolution Explorer (GALEX) is a NASA Small Explorer, launched in 2003 April, developed in cooperation with the Centre National d’Études Spatiales of France and the Korean Ministry of Science and Technology.

Funding for the SDSS and SDSS-II has been provided by the Alfred P. Sloan Foundation, the Participating Institutions, the National Science Foundation, the US Department of Energy, the National Aeronautics and Space Administration, the Japanese Monbukagakusho, the Max Planck Society, and the Higher Education Funding Council for England. The SDSS website is <http://www.sdss.org/>.

JF acknowledges the support from the National Science Foundation of China no. 11173044 and the Shanghai Committee of Science and Technology grant no. 12ZR1452700.

MA acknowledges support from the DFG Excellence Cluster ‘Origin and Structure of the Universe’.

REFERENCES

- Abazajian K. N. et al., 2009, *ApJS*, 182, 543
- Aumer M., White S. D., 2013, *MNRAS*, 428, 1055
- Aumer M., White S. D., Naab T., Scannapieco C., 2013, *MNRAS*, 434, 3142
- Bigiel F., Blitz L., 2012, *ApJ*, 756, 183 (B12)
- Bigiel F., Leroy A., Walter F., Brinks E., de Blok W. J. G., Madore B., Thornley M. D., 2008, *AJ*, 136, 2846
- Blitz L., Rosolowsky E., 2006, *ApJ*, 650, 933
- Bosma A., 1978, PhD thesis, Groningen University
- Broeils A. H., Rhee M.-H., 1997, *A&A*, 324, 877
- Bullock J. S., Dekel A., Kolatt T. S., Kravtsov A. V., Klypin A. A., Porciani C., Primack J. R., 2001, *ApJ*, 555, 240
- Catinella B., Schiminovich D., Kauffmann G., Fabello S., Wang J., 2010, *MNRAS*, 403, 683 (C10)
- Cayatte V., van Gorkom J. H., Balkowski C., Kotanyi C., 1990, *AJ*, 100, 604

- Cayatte V., Kotanyi C., Balkowski C., van Gorkom J. H., 1994, *AJ*, 107, 1003
- Chung A., van Gorkom J. H., Kenney J. D. P., Crowl H., Vollmer B., 2009, *AJ*, 138, 1741
- Conselice C., 2003, *ApJS*, 147, 1
- Dutton A. A., van den Bosch F. C., Dekel A., Courteau S., 2007, *ApJ*, 654, 27
- Elmegreen B. G., 1993, *ApJ*, 411, 170
- Fu J., Hou J. L., Yin J., Chang R. X., 2009, *ApJ*, 696, 668
- Fu J., Guo Q., Kauffmann G., Krumholz M. R., 2010, *MNRAS*, 409, 515
- Fu J. et al., 2013, *MNRAS*, 1755 (Fu13)
- Guo Q. et al., 2011, *MNRAS*, 413, 101
- Jarrett T. H. et al., 2011, *ApJ*, 735, 112
- Jarrett T. H. et al., 2013, *AJ*, 145, 6
- Kauffmann G., 1996, *MNRAS*, 281, 475
- Leroy A. K., Walter F., Brinks E., Bigiel F., de Blok W. J. G., Madore B., Thornley M. D., 2008, *AJ*, 136, 2782
- Lotz J. M., Primack J., Madau P., 2004, *AJ*, 613, 262
- Markwardt C. B., 2009, in David A., Bohlender D. D., Patrick D., eds, *ASP Conf. Ser. Vol. 411, Astronomical Data Analysis Software and Systems XVIII*. Astron. Soc. Pac., San Francisco, p. 251
- Martin A. M., Papastergis E., Giovanelli R., Haynes M. P., Springob C. M., Stierwalt S., 2010, *ApJ*, 723, 1359
- Martinsson T. P. K., 2011, PhD thesis, chapter 4, p. 140, available at: <http://irs.ub.rug.nl/ppn/339227109>
- Martinsson T. P. K., Verheijen M. A. W., Westfall K. B., Bershadsky M. A., Andersen D. R., Swaters R. A., 2013, *A&A*, 557, 131
- Mo H. J., Mao S., White S. D. M., 1998, *MNRAS*, 295, 319
- Noordermeer E., van der Hulst J. M., Sancisi R., Swaters R. A., van Albada T. S., 2005, *A&A*, 442, 137
- Obreschkow D., Croton D., de Lucia G., Khochfar S., Rawlings S., 2009, *ApJ*, 698, 1467
- Salim S. et al., 2007, *ApJS*, 173, 267
- Swaters R. A., van Albada T. S., van der Hulst J. M., Sancisi R., 2002, *A&A*, 390, 829
- van der Hulst J. M., van Albada T. S., Sancisi R., 2001, in Hibbard J. E., Rupen M., van Gorkom J.H., eds, *ASP Conf. Ser. Vol. 240, Astron. Soc. Pac., San Francisco*, p. 451
- Verheijen M. A. W., Sancisi R., 2001, *A&A*, 370, 765
- Wang J. et al., 2013, *MNRAS*, 433, 270 (Paper I)
- Warmels R. H., 1988, *A&AS*, 72, 19
- Wevers B. M. H. R., Appleton P. N., Davies R. D., Hart L., 1984, *A&A*, 140, 125
- Wright E. L. et al., 2010, *AJ*, 140, 1868

This paper has been typeset from a \TeX/L\AA\TeX file prepared by the author.